nature COMMUNICATIONS

ARTICLE

Received 18 Jul 2013 | Accepted 7 Nov 2013 | Published 11 Dec 2013

DOI: 10.1038/ncomms3893

5*d* iridium oxide as a material for spin-current detection

Kohei Fujiwara[1,†], Yasuhiro Fukuma[1,†], Jobu Matsuno[1,†], Hiroshi Idzuchi[2], Yasuhiro Niimi[2], YoshiChika Otani[1,2,†] & Hidenori Takagi[1,3]

Devices based on pure spin currents have been attracting increasing attention as key ingredients for low-dissipation electronics. To integrate such spintronics devices into charge-based technologies, electric detection of spin currents is essential. The inverse spin Hall effect converts a spin current into an electric voltage through spin-orbit coupling. Noble metals such as Pt and Pd, and also Cu-based alloys, have been regarded as potential materials for a spin-current injector, owing to the large direct spin Hall effect. Their spin Hall resistivity ρ_{SH}, representing the performance as a detector, is not large enough, however, due mainly because of their low charge resistivity. Here we report that a binary 5*d* transition metal oxide, iridium oxide, overcomes the limitations encountered in noble metals and Cu-based alloys and shows a very large $\rho_{SH} \sim 38\,\mu\Omega\,$cm at room temperature.

[1] RIKEN Advanced Science Institute, Wako, Saitama 351-0198, Japan. [2] Institute for Solid State Physics, University of Tokyo, Kashiwa, Chiba 277-8581, Japan. [3] Department of Physics, University of Tokyo, Hongo, Tokyo 113-0033, Japan. † Present addresses: The Institute of Scientific and Industrial Research, Osaka University, Ibaraki, Osaka 567-0047, Japan. (K.F.); Frontier Research Academy for Young Researchers, Kyushu Institute of Technology, Iizuka, Fukuoka 820-8502, Japan. (Y.F.); RIKEN Center for Emergent Matter Science (CEMS), Wako, Saitama 351-0198, Japan. (J.M., Y.O.). Correspondence and requests for materials should be addressed to K.F. (email: kfujiwara@sanken.osaka-u.ac.jp).

Spin-orbit coupling (SOC) is a relativistic effect and relates the spin moment of an electron to its orbital momentum via a momentum-dependent effective magnetic field. In the presence of SOC, a charge current without any spin polarization can be converted into a pure spin current (the flow of spin angular momentum) and *vice versa*, known as the direct spin Hall effect and the inverse spin Hall effect (ISHE)[1–18]. The presence of these phenomena in non-magnetic semiconductors had already been recognized in 1970s (refs 19–22) but recent theoretical[1,2] and experimental investigations[3,4] have given a boost to this field. Spin current-based electronics with low-energy consumption has since been discussed, where spin-current injection and detection, using charge/spin conversion by direct spin Hall effect and ISHE, played a key role. A variety of materials have subsequently been explored to realize efficient charge/spin conversion[5–18]. The playground for the exploration was first limited to semiconductors but then extended to metals, where we can take advantage of the less pronounced effect of interfacial barriers. Heavy transition metals such as Pt[6–10,14], Au[9,12,13], and Pd[8,9,11] and also Cu-based alloys[17,18] were found to exhibit a particularly large spin Hall angle α_{SH} (the maximum yield of the charge/spin conversion), 0.01–0.1 at room temperature, owing to their pronounced SOC effects. These effects give these metals an advantage for application as a spin injector. In addition to the large α_{SH}, their low electrical resistivity (ρ_C), typically $\rho_C = 10^{-7}$–$10^{-5}\,\Omega$ cm, allows large charge currents to be passed and hence to inject a large spin current without serious Joule heating.

Spin currents can be detected by using the ISHE. In contrast to the case for spin injectors, the low ρ_C of the heavy metals with a large α_{SH} is a disadvantages when it comes to spin detection. In the ISHE, the electric voltage ΔV_{ISHE} generated by a spin current I_S is in proportion to ρ_C (refs 23,24):

$$\Delta V_{ISHE} \propto \alpha_{SH}\rho_C I_S \approx \rho_{SH} I_S. \quad (1)$$

Spin Hall resistivity given by $\rho_{SH} \approx \alpha_{SH}\rho_C$ determines the efficiency of spin-current detection. This means that a sensitive detection of spin current could be achieved in materials with both a large α_{SH} and a high ρ_C. In typical heavy metals, their low ρ_C imposes strong constraints in tuning the value of ρ_{SH} as it remains as low as $<1\,\mu\Omega$ cm. One of the obvious approaches to improve the performance of spin detectors could be to increase the ρ_C by alloying. Alloying can in fact increase not only the ρ_C but also the α_{SH} through an extrinsic spin Hall effect[25–27]. At room temperature where the inelastic scattering of charge carriers is dominant, however, it should be hard to anticipate a drastic increase of ρ_C by alloying, for example, more than an order of magnitude increase as compared with the pristine material. Therefore, the improvement of ρ_{SH} would not be achieved only by alloying.

In this work, we propose 5*d* transition metal oxides (TMOs) as alternative metals to realize both large α_{SH} and large ρ_C, which should enhance ρ_{SH}. The uniqueness of 5*d* TMOs is characterized by the extremely strong SOC $\sim$0.5–1 eV originating from the predominant 5*d* character of the conduction band. The SOC in 5*d* TMOs is in fact as strong as to reconstruct the electronic structures drastically, as first discussed in the case of $J_{eff} = 1/2$ Mott state Sr_2IrO_4 (ref. 28). The analogous predominant SOC effect has been commonly observed in a broad range of Ir oxides including Ba_2IrO_4 (ref. 29), $CaIrO_3$ (ref. 30) and Ir_2O_4 (ref. 31). In those Ir oxides, in addition to the strong SOC, the localized character of *d* orbitals gives rise to a moderately high charge resistivity ρ_C even in the metallic state. Typical ρ_C values of conductive 5*d* Ir TMOs such as IrO_2 and $SrIrO_3$ at room temperature are of the order of 10^{-4}–$10^{-3}\,\Omega$ cm, at least one order of magnitude higher than those of normal *s* metals. As the variety of materials continues to grow rapidly, 5*d* TMOs offer a unique opportunity to explore the giant ρ_{SH} for efficient spin detection. We selected a simple binary oxide, rutile IrO_2 (refs 32–34), as the basis for our exploration. IrO_2 with Ir^{4+} shares the same $5d^5$ configuration with many other Ir oxides, where the strong SOC dominates the electronic states and the resultant electronic properties[34]. This binary oxide has been long used as an electrode in various device applications, ranging from non-volatile ferroelectric memories to electrochemical devices. The excellent electrode properties are due to the formation of a clean, well-defined interface with other materials owing to its high chemical and thermal stability, and superior barrier properties for oxygen diffusion. In such a clean interface, it may be possible to inject a spin current through a diffusion process; IrO_2 is therefore an ideal platform for testing the ISHE of 5*d* TMOs. Here, we describe successful spin-current injection into IrO_2 using a lateral spin-valve (LSV) device geometry and demonstrate the ISHE with a remarkably high ρ_{SH} as a metal not only in the polycrystalline state but also in the practically important amorphous state.

Results

Device structure. We fabricated cross-junction-type devices consisting of an IrO_2 wire and a permalloy($Ni_{80}Fe_{20}$, Py)/Ag/Py LSV[35], shown in Fig. 1a,b (see also Methods). Spin currents are passed in the Ag strip by a non-local charge current injection (I_C) from the ferromagnetic Py electrode and are perpendicularly injected in part into the IrO_2 wire through the diffusion (Fig. 1a). This effect, called spin absorption, enables us to conduct a quantitative analysis of the ISHE as have been demonstrated for various materials[7,8,17,18]. We examined the potential of polycrystalline and amorphous IrO_2 wires as the spin detector element. Their resistivities were $2.0 \times 10^{-4}\,\Omega$ cm and $5.7 \times 10^{-4}\,\Omega$ cm at 300 K, respectively, which are 1–2 orders of magnitude higher than those of metals that have been studied to date as a spin Hall material.

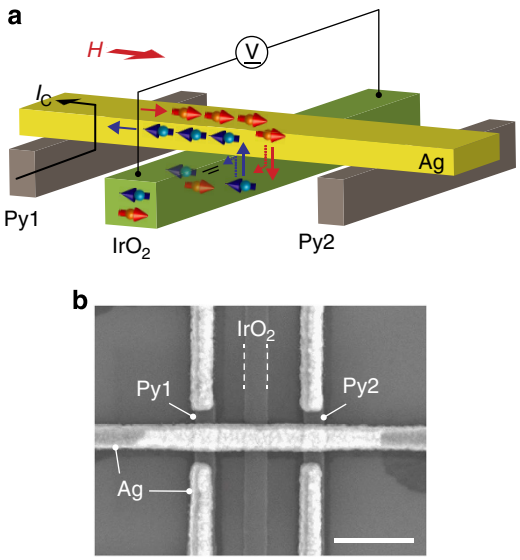

Figure 1 | Inverse spin Hall effect measurements using a spin absorption effect in a lateral spin-valve geometry. (**a**) The structure of device used for ISHE measurements is shown schematically. A LSV with two Py electrodes (Py1: spin source, Py2: spin detector) bridged by an Ag spin transport layer was formed on an IrO_2 wire. Spin-polarized charge current, I_C, was injected along the arrow to accumulate pure spin currents in the Ag. The diffusion of spin current into the IrO_2 wire, namely, the spin absorption, gives rise to the ISHE in IrO_2. (**b**) Scanning electron microscopy image of a typical device. Scale bar, 500 nm. The dotted lines indicate the side edges of the IrO_2 wire for clarity.

To check that the Ag layer is not oxidized by directly contacting with IrO_2, we first characterized the Ag/IrO_2 interface by means of interface resistance measurements[36]. The current–voltage characteristics of the Ag/IrO_2 interface showed an ohmic behaviour, typical of metal/metal interface. The slope of the data yielded a resistance–area product (RA) of 2.3 fΩ m^2 at 300 K, which is as low as that of the metallic, transparent Ag/Py interface (RA = 1.9 fΩ m^2 at 300 K). An estimate of the thickness of the possibly oxidized Ag layer, using the resistivities of Ag_2O and AgO in the literature[37], never exceeded 0.1 nm. These observations imply that the Ag/IrO_2 interface in the present devices is very sharp as in metal/metal interfaces.

Spin-current injection into IrO_2. The spin absorption by IrO_2 across the interface was then confirmed by non-local spin-valve (NLSV) experiments[7,8,17,18,35]. The schematic diagram of the measurement is shown in Fig. 2a. The pure spin currents accumulated in the Ag strip by injecting spin-polarized charge currents I_C from Py1 to Ag is detected as a voltage V_S ($=V_+ - V_-$) between Py2 (V_+) and Ag (V_-) (upper panel). The spin accumulation signal ΔR_S is given by the difference in V_S/I_C (R_S) between parallel (high R_S) and antiparallel (low R_S) magnetizations of the two Py wires. If an IrO_2 middle wire is in contact with the Ag, the accumulated spin diffuses in part into it (lower panel), resulting in the reduction in ΔR_S (ref. 7). Figure 2b and c show field dependences of R_S at 300 and 10 K, respectively. The decrease of ΔR_S by the insertion of the IrO_2 middle wire indicates the spin absorption effect. This is more clearly demonstrated in the *t*emperature (T) dependence of ΔR_S with (ΔR_S^{with}) and without ($\Delta R_S^{without}$) the middle wire, as displayed in Fig. 2d. At all the temperatures, ΔR_S^{with} is systematically smaller than $\Delta R_S^{without}$, while both are enhanced at low temperatures owing to the increase of the spin-diffusion length of Ag (λ_{Ag})[35]. By analysing the data based on the three-dimensional spin-diffusion model[18] (see Supplementary Methods and Supplementary Fig. S1), we estimated a spin-diffusion length in polycrystalline IrO_2, $\lambda_{IrO_2} = 3.8$ nm at 300 K and 8.4 nm at 10 K, which are comparable to those of Pt (3–10 nm at 300 K (refs 6–10,14)) and CuIr (5–20 nm at 10 K (ref. 17)) where relatively large spin Hall angles were observed. This indicates that spin scattering of IrO_2 is indeed very strong as expected from the 5*d* conduction band[34].

ISHE and ρ_{SH} of IrO_2. By injecting spin currents through the spin absorption effect, we successfully observed ISHE in IrO_2. In Fig. 3a,b, we plot the room-temperature ISHE signal R_{ISHE} ($\equiv \Delta V_{ISHE}/I_C$) for polycrystalline and amorphous samples as a function of the magnetic field (The temperature dependence of the ISHE is shown in Supplementary Fig. S2 and is explained in Supplementary Note 1). Here the magnetic field was applied along the hard axis of the Py spin source (see Fig. 1a), and ΔV_{ISHE} was induced along the long-axis direction of the IrO_2 wire. Reflecting the magnetization process in hard axis of Py, R_{ISHE} linearly increased up to ~1,500 Oe and then saturated. The antisymmetric response to the applied magnetic field excludes any spurious effects such as anisotropic magnetoresistance of Py; the ISHE of IrO_2 is responsible for the resistance change ($2\Delta R_{ISHE}$) between positive and negative magnetic fields. The in-plane angular dependence of magnetic field effect on R_{ISHE} was confirmed fully consistent with the ISHE origin. Figure 3c shows the variation in R_{ISHE} under a magnetic field direction rotated by ϕ with respect to the ordinary set-up (Fig. 3d, inset). The sign change of R_{ISHE} occurs between $\phi = 0$ and π by magnetization switching of Py and concomitant polarization reversal of the spin

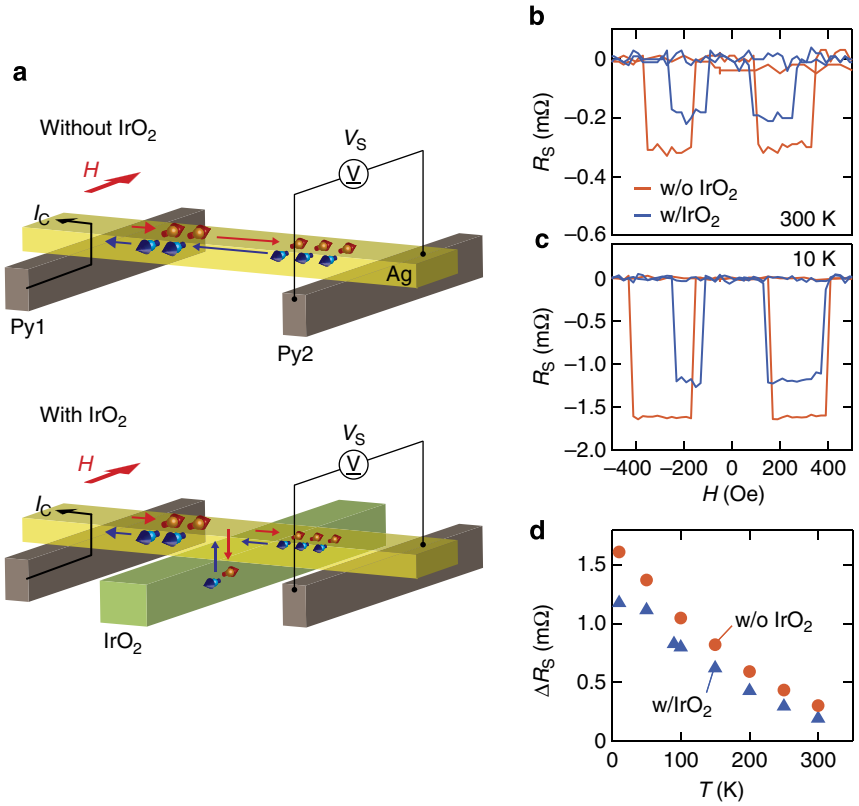

Figure 2 | Non-local spin-valve measurements. (**a**) The set-up of measurement is schematically depicted. The magnetic field H is applied along the easy axis of the Py electrodes. (**b**,**c**) NLSV signals measured at 300 K and 10 K for Py/Ag/Py LSVs without and with the polycrystalline IrO_2 middle wire. (**d**) Temperature dependences of the NLSV signals.

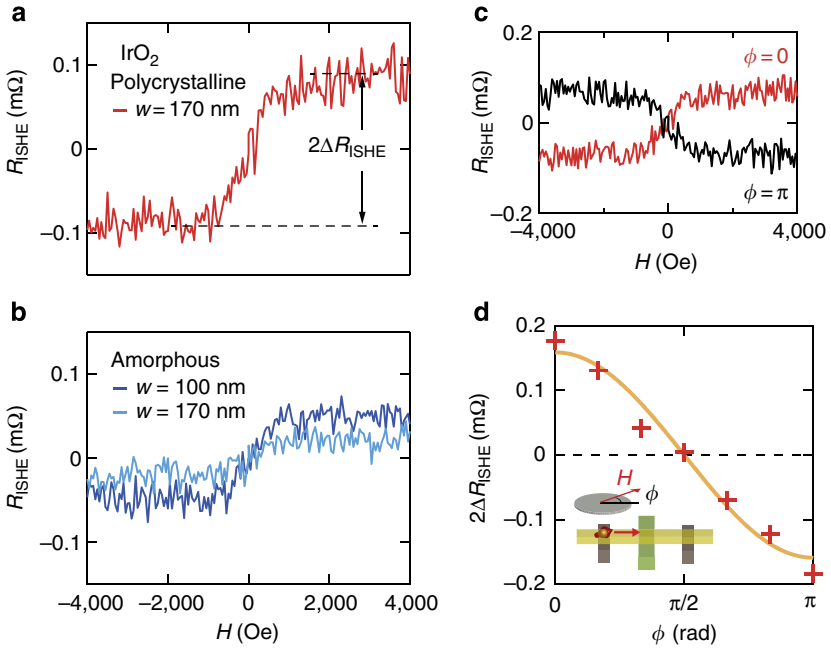

Figure 3 | Inverse spin Hall effect of IrO_2 at 300 K. (**a**) The ISHE signal R_{ISHE} ($\equiv \Delta V_{ISHE}/I_C$) for a polycrystalline IrO_2 wire with a width w of 170 nm was measured as a function of the applied magnetic field H. (**b**) The results for amorphous IrO_2 samples. Two devices with different w values (100 and 170 nm) were measured. The 100 nm-width device showed larger R_{ISHE} because of the increase of spin-current density. R_{ISHE} of the two amorphous devices are smaller than that of the polycrystalline sample shown in **a**. (**c**,**d**) Angular dependence of R_{ISHE} and the resistance change $2\Delta R_{ISHE}$ by the ISHE. The in-plane azimuthal angle ϕ with respect to the long axis of Ag is rotated to change the polarization direction of the spin current (inset in **d**). The solid line in **d** is a $\cos\phi$ curve fitted to the results.

current. As shown in Fig. 3d, the resistance change $2\Delta R_{ISHE}$ vanishes at $\phi = \pi/2$ and exhibits a $\cos\phi$ relation. This characteristic angular dependence is the hallmark of ISHE[7,12], evidencing spin-dependent electron scattering in IrO_2.

Because of the large difference in ρ_C between Ag and IrO_2, the charge current induced in the IrO_2 wire by the ISHE is partially shunted by the adjacent Ag layer. To take into account such geometric effects and to precisely determine ρ_{SH}, we adopted the three-dimensional spin-diffusion model (see also Supplementary Methods). Using the ISHE signal $2\Delta R_{ISHE}$ and data obtained from the NLSV measurements, α_{SH} and ρ_{SH} are, respectively, calculated to be 0.040 and 8.0 μΩ cm for polycrystalline IrO_2, and 0.065 and 37.5 μΩ cm for amorphous IrO_2 at 300 K.

Figure 4 summarizes spin Hall resistivity ρ_{SH} and electrical resistivity ρ_C for a variety of metals with a large spin Hall angle α_{SH} reported so far, together with that for IrO_2. It mimics the point of this work in that ρ_{SH} of IrO_2 is distinctly large compared with typical heavy metals and their alloys of which ρ_{SH} is ~0.16–1.2 μΩ cm (refs 6–14,17,18), and is now comparable to the large ρ_{SH} that was recently discovered in ultrathin films of β-phase (A15 crystal structure) W (ref. 15) and Ta (ref. 16).

Discussion

To generate a large electric voltage using the ISHE of IrO_2 from existing metal-based spin-current devices, it is important to reduce the shunting effect at the Ag/IrO_2 interface due to their large difference in ρ_C. One of the promising approaches is to use Al (ref. 38) and Mg (ref. 39) as the non-magnetic spin transport layer. Their ρ_C values are one order of magnitude higher than that of Ag we used, of the order of 10 μΩ cm at room temperature, while a comparably long spin-diffusion length is obtained. Another interesting route is a spin transport layer based on a conductive oxide composed of light elements with small SOC. For example, in ZnO (ref. 40), doping with Al yields ρ_C of the order of 100 μΩ cm (ref. 41), which can match with that of IrO_2. The high chemical stability of IrO_2 could be advantageous in fabricating such oxide-based junctions.

The discovery of the ISHE in amorphous IrO_2, which can be grown at room temperature, is a significant step towards spintronics devices based on such oxide materials. The comparably large α_{SH} in the amorphous form may point to that spin scattering in this compound occurs at the length scale of as short as a unit cell, potentially enabling the spin detection at the atomic layer thickness. Although the physics of spin scattering in amorphous states has not been understood yet, the availability of the amorphous form should make it easier to study SOC-induced transport phenomena in 5*d* TMOs not used before in spintronics.

In conclusion, 5*d* TMOs are the most promising materials for spin detection in spintronics. We demonstrated that the combination of strong SOC and a moderately high ρ_C is a key to improve the performance of spin detection. These achievements in the simple binary oxide manifest the potential of 5*d* TMOs as a new class of spintronic materials. Strong SOC in this class of materials produces a rich variety of intriguing physical properties, including correlated topological insulator[42], Weyl semi-metal[43] and Kitaev spin liquid[44]. Our discovery of the large spin Hall resistivity may make 5*d* TMOs even more fascinating.

Methods

Device fabrication. The Py/Ag/Py LSV with an IrO_2 middle wire was fabricated on a SiO_2/Si substrate. Au/Ti leads for electrical measurements were prepared on the substrate by a photolithography and an e-beam deposition. IrO_2 film was grown by a reactive sputtering with a 99.9% pure Ir target. A wire structure of IrO_2 was formed using a posi-type resist patterned by an e-beam lithography. The typical wire width and thickness were 170 and 15 nm, respectively. During the deposition, the substrate was not heated, and the pressure was fixed at 0.7 Pa of Ar/O_2 (90:10) mixture gas. X-ray diffraction analysis indicated that the as-deposited IrO_2 film was amorphous. The amorphous film turned into

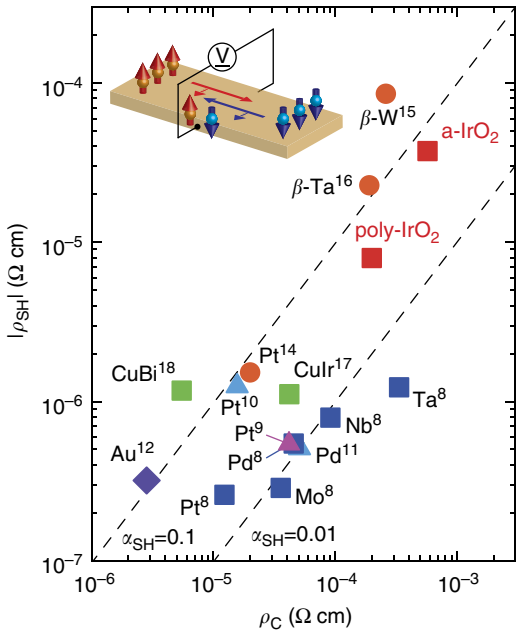

Figure 4 | Spin Hall resistivity of metals. Experimentally measured values of spin Hall resistivity ρ_{SH} for various metals are plotted as a function of electrical resistivity ρ_C. Data include Pt (refs 9,10) and Pd (ref. 11) evaluated at room temperature by spin pumping, Pt (ref. 14) and atomic layer thin films of β-W (ref. 15) and β-Ta (ref. 16) at room temperature by spin-transfer-torque ferromagnetic resonance, Au at 295 K using a planar Hall device[12], Ta, Nb, Pd, Mo, Pt (ref. 8), 12% Ir-doped Cu (ref. 17), 0.5% Bi-doped Cu (ref. 18) at 10 K, and polycrystalline and amorphous IrO_2 at 300 K (this work) by spin absorption.

polycrystalline after a post-annealing at 400 °C in air. The LSV with a Py–Py separation of 700 nm (centre-to-centre) was then formed onto the IrO_2 wire by the shadow evaporation method[35,36]. To prevent the surface oxidation of Ag, a 2-nm-thick MgO protection layer was e-beam deposited on the surface without breaking vacuum. The width and thickness of wire were 170 and 100 nm for Ag, and 170 and 20 nm for Py, respectively. Their ρ_C and spin-diffusion length were 3.0 μΩ cm and 330 nm for Ag and 47 μΩ cm and 5 nm for Py, respectively, at 300 K. One of the two Py electrodes was made longer than the other (not shown in Fig. 1b) to make the contrast in the fields for magnetization reversal.

Electrical measurements. All electrical measurements were performed by a standard lock-in technique in a He flow cryostat. An alternating current I_C of 200 μA with a frequency of 79 Hz was used for NLSV measurements. In ISHE measurements, I_C of 400 μA was applied. We confirmed the linearity between the output voltage ΔV_{ISHE} and I_C in the range of 100–400 μA.

References

1. Hirsch, J. Spin Hall effect. *Phys. Rev. Lett.* **83,** 1834–1837 (1999).
2. Zhang, S. Spin Hall effect in the presence of spin diffusion. *Phys. Rev. Lett.* **85,** 393–396 (2000).
3. Kato, Y. K., Myers, R. C., Gossard, A. C. & Awschalom, D. D. Observation of the spin Hall effect in semiconductors. *Science* **306,** 1910–1913 (2004).
4. Wunderlich, J., Kaestner, B., Sinova, J. & Jungwirth, T. Experimental observation of the spin-Hall effect in a two-dimensional spin-orbit coupled semiconductor system. *Phys. Rev. Lett.* **94,** 047204 (2005).
5. Valenzuela, S. O. & Tinkham, M. Direct electronic measurement of the spin Hall effect. *Nature* **442,** 176–179 (2006).
6. Saitoh, E., Ueda, M., Miyajima, H. & Tatara, G. Conversion of spin current into charge current at room temperature: inverse spin-Hall effect. *Appl. Phys. Lett.* **88,** 182509 (2006).
7. Kimura, T., Otani, Y., Sato, T., Takahashi, S. & Maekawa, S. Room-temperature reversible spin Hall effect. *Phys. Rev. Lett.* **98,** 156601 (2007).
8. Morota, M. *et al.* Indication of intrinsic spin Hall effect in 4d and 5d transition metals. *Phys. Rev. B* **83,** 174405 (2011).
9. Mosendz, O. *et al.* Detection and quantification of inverse spin Hall effect from spin pumping in permalloy/normal metal bilayers. *Phys. Rev. B* **82,** 214403 (2010).
10. Ando, K. *et al.* Electric manipulation of spin relaxation using the spin Hall effect. *Phys. Rev. Lett.* **101,** 036601 (2008).
11. Ando, K. & Saitoh, E. Inverse spin-Hall effect in palladium at room temperature. *J. Appl. Phys.* **108,** 113925 (2010).
12. Seki, T. *et al.* Giant spin Hall effect in perpendicularly spin-polarized FePt/Au devices. *Nat. Mater.* **7,** 125–129 (2008).
13. Mihajlović, G., Pearson, J., Garcia, M., Bader, S. & Hoffmann, A. Negative nonlocal resistance in mesoscopic gold Hall bars: absence of the giant spin Hall effect. *Phys. Rev. Lett.* **103,** 166601 (2009).
14. Liu, L., Moriyama, T., Ralph, D. & Buhrman, R. Spin-torque ferromagnetic resonance induced by the spin Hall effect. *Phys. Rev. Lett.* **106,** 036601 (2011).
15. Pai, C.-F. *et al.* Spin transfer torque devices utilizing the giant spin Hall effect of tungsten. *Appl. Phys. Lett.* **101,** 122404 (2012).
16. Liu, L. *et al.* Spin-torque switching with the giant spin Hall effect of tantalum. *Science* **336,** 555–558 (2012).
17. Niimi, Y. *et al.* Extrinsic spin Hall effect induced by iridium impurities in copper. *Phys. Rev. Lett.* **106,** 126601 (2011).
18. Niimi, Y. *et al.* Giant spin Hall effect induced by skew scattering from bismuth impurities inside thin film CuBi alloys. *Phys. Rev. Lett.* **109,** 156602 (2012).
19. Chazalviel, J.N. & Solomon, I. Experimental evidence of the anomalous Hall effect in a nonmagnetic semiconductor. *Phys. Rev. Lett.* **29,** 1676–1679 (1972).
20. Chazalviel, J.N. Spin-dependent Hall effect in semiconductors. *Phys. Rev. B* **11,** 3918–3934 (1975).
21. D'yakonov, M. I. & Perel', V. I. Possibilty of orienting electron spins with current. *Sov. Phys. JETP Lett.* **13,** 467–469 (1971).
22. Bakun, A. A., Zakharchenya, B. P., Rogachev, A. A., Tkachuk, M. N. & Fleisher, V. G. Observation of a surface photocurrent caused by optical orientation of electons in a semiconductor. *Sov. Phys. JETP Lett.* **40,** 1293–1295 (1984).
23. Ando, K. & Saitoh, E. Observation of the inverse spin Hall effect in silicon. *Nat. Comm.* **3,** 629 (2012).
24. Vila, L., Kimura, T. & Otani, Y. Evolution of the spin Hall effect in Pt nanowires: size and temperature effects. *Phys. Rev. Lett.* **99,** 226604 (2007).
25. Gu, B. *et al.* Surface-assisted spin Hall effect in Au films with Pt impurities. *Phys. Rev. Lett.* **105,** 216401 (2010).
26. Fert, A. & Levy, P. Spin Hall effect induced by resonant scattering on impurities in metals. *Phys. Rev. Lett.* **106,** 157208 (2011).
27. Gradhand, M. *et al.* Perfect alloys for spin Hall current-induced magnetization switching. *SPIN* **2,** 1250010 (2012).
28. Kim, B. J. *et al.* Phase-sensitive observation of a spin-orbital Mott state in Sr_2IrO_4. *Science* **323,** 1329–1332 (2009).
29. Okabe, H. *et al.* Ba_2IrO_4: a spin-orbit Mott insulating quasi-two-dimensional antiferromagnet. *Phys. Rev. B* **83,** 155118 (2011).
30. Ohgushi, K. *et al.* Resonant X-ray diffraction study of strongly spin-orbit-coupled Mott insulator $CaIrO_3$. *Phys. Rev. Lett.* **110,** 217212 (2013).
31. Kuriyama, H. *et al.* Epitaxially stabilized iridium spinel oxide without cations in the tetrahedral site. *Appl. Phys. Lett.* **96,** 182103 (2010).
32. Ryden, W., Lawson, A. & Sartain, C. Electrical transport properties of IrO_2 and RuO_2. *Phys. Rev. B* **1,** 1494–1500 (1970).
33. Mattheiss, L. Electronic structure of RuO_2, OsO_2, and IrO_2. *Phys. Rev. B* **13,** 2433–2450 (1976).
34. Hirata, Y. *et al.* Complex orbital state stabilized by strong spin-orbit coupling in a metallic iridium oxide IrO_2. *Phys. Rev. B* **87,** 161111 (2013).
35. Idzuchi, H., Fukuma, Y., Wang, L. & Otani, Y. Spin relaxation mechanism in silver nanowires covered with MgO protection layer. *Appl. Phys. Lett.* **101,** 022415 (2012).
36. Fukuma, Y. *et al.* Giant enhancement of spin accumulation and long-distance spin precession in metallic lateral spin valves. *Nat. Mater.* **10,** 527–531 (2011).
37. Abe, Y., Hasegawa, T., Kawamura, M. & Sasaki, K. Characterization of Ag oxide thin films prepared by reactive RF sputtering. *Vacuum* **76,** 1–6 (2004).
38. Valenzuela, S. O. & Tinkham, M. Spin-polarized tunneling in room-temperature mesoscopic spin valves. *Appl. Phys. Lett.* **85,** 5914 (2004).
39. Idzuchi, H., Fukuma, Y., Wang, L. & Otani, Y. Spin diffusion characteristics in magnesium nanowires. *Appl. Phys. Express* **3,** 063002 (2010).
40. Althammer, M., Karrer-Müller, E.-M., Goennenwein, S. T. B., Opel, M. & Gross, R. Spin transport and spin dephasing in zinc oxide. *Appl. Phys. Lett.* **101,** 082404 (2012).
41. Suzuki, A., Matsushita, T., Wada, N., Sakamoto, Y. & Okuda, M. Transparent conducting Al-doped ZnO thin films prepared by pulsed laser deposition. *Jpn J. Appl. Phys.* **35,** L56–L59 (1996).
42. Shitade, A. *et al.* Quantum spin Hall effect in a transition metal oxide Na_2IrO_3. *Phys. Rev. Lett.* **102,** 256403 (2009).
43. Wan, X., Turner, A. M., Vishwanath, A. & Savrasov, S. Y. Topological semimetal and Fermi-arc surface states in the electronic structure of pyrochlore iridates. *Phys. Rev. B* **83,** 205101 (2011).
44. Jackeli, G. & Khaliullin, G. Mott insulators in the strong spin-orbit coupling limit: from Heisenberg to a quantum compass and Kitaev models. *Phys. Rev. Lett.* **102,** 017205 (2009).

Acknowledgements
We thank K. Ohgushi for helpful discussions. This work was supported by Grants-in-Aid (number 22340108, 23103518 and 24224010) from MEXT, Japan.

Author contributions
K.F., Y.F. and J.M. designed the experiments. K.F., Y.F. and H.I. fabricated devices and collected the data. K.F. and Y.N. analysed the data. K.F. wrote the manuscript with input from J.M. Y.O., and H.T. H.T. and Y.O. planned and supervised the project. All authors discussed the results.

Additional information
Supplementary Information accompanies this paper at http://www.nature.com/naturecommunications

Competing financial interests: The authors declare no competing financial interests.

Reprints and permission information is available online at http://npg.nature.com/reprintsandpermissions/

How to cite this article: Fujiwara, K. *et al.* 5*d* iridium oxide as a material for spin-current detection. *Nat. Commun.* 4:2893 doi: 10.1038/ncomms3893 (2013).